

lower transition region ($\sim 6,000 - 40,000$ K), respectively (Vernazza, Avrett, and Loeser 1973, 1981; Fontenla, Avrett, and Loeser 1991). In these quiescent conditions, the varied formation heights of different parts of the line wings have been suggested as a diagnostic of density and temperature across the chromosphere (Roussel-Dupre 1983). However, due to long thermalisation lengths, each wavelength of the Ly α line samples a range of temperatures, limiting it to a secondary diagnostic. These formation conditions undergo drastic changes during flares, as large amounts of energy are deposited into the chromosphere. Flare modelling by Hong et al. (2019) demonstrated that the formation heights of the Ly α line profile vary significantly between different models. In most flare models driven by nonthermal heating, the Ly α line wings and core form at distinct heights within the chromosphere, both of which are lower than their formation heights under quiescent conditions. This behaviour was attributed to decreasing opacity to wing photons as neutral hydrogen above is excited, with the conditions above the core remaining similar to preflare conditions. However, models with relatively more low-energy nonthermal electrons, as well as a model driven by thermal conduction, showed the wings and core forming at the same height, in the middle chromosphere. This was due to a condensation layer, which lowered the formation region, while the material above was transparent due to significant ionisation. These changes to the line's formation should be considered when interpreting spectrally resolved Ly α flare observations.

Observations show that different processes during flares can drive enhancement of Ly α in both the chromosphere and corona. In the chromosphere, Ly α enhancement may result from the thermalisation of flare-accelerated electrons with ambient material, where Coulomb collisions excite neutral hydrogen, leading to increased Ly α emission via radiative de-excitation (Kurokawa, Takakura, and Ohki 1988). However, observations from the Ly α channel of the Extreme Ultraviolet Imager's High-Resolution Imager on Solar Orbiter (SolO/EUI HRILy α ; Müller et al. 2020; Rochus et al. 2020) reveal a more elaborate scenario. Li et al. (2022) analysed a C-class flare, finding Ly α emission to originate from both flare ribbons and loops. The study demonstrated a strong temporal correlation between Ly α and SXR emission, the primary source of Ly α emission being flare ribbons. Due to this, the authors suggested the Ly α enhancement was predominantly driven by the conduction of energy from coronal flare loops to the chromosphere. Additionally, Hard X-ray (HXR) emission driven by the injection of nonthermal energy was cospatial with these Ly α ribbons, indicating that this injection further contributed to Ly α enhancement. Additional Ly α emission was observed in flare loops, likely driven by the radiative cooling of hot plasma in these structures. Ly α imaging observations of an M-class flare and filament eruption from the Transition Region and Coronal Explorer (TRACE; Handy et al. 1999) were reported by Rubio da Costa et al. (2009). Their analysis demonstrated that Ly α emission originated primarily from flare footpoints and was cospatial with HXR sources, leading the authors to suggest these Ly α enhancements were driven by nonthermal heating of the chromosphere. Further evidence of Ly α flare enhancement associated with filament-eruptions was provided by Wauters et al. (2022), who analysed an M6.7 flare with photometric Ly α observations from the Large Yield Radiometer (LYRA) on the Project for On-Board Autonomy 2 (PROBA-2; Dominique et al. 2013). Their studies revealed emission from a bright filament-eruption captured in 1600 Å images from the Solar Dynamics Observatory's Atmospheric Imaging Assembly (SDO/AIA; Pesnell, Thompson, and Chamberlin 2012; Lemen et al. 2012) that correlated with gradual phase Ly α enhancements, suggesting the filament-eruption may have contributed significantly to Ly α enhancement in this event.

The spectral properties of Ly α during flares remain insufficiently studied, resulting in limited information on how spectral variability (e.g. line asymmetry, variation in enhancements of different regions of the line) varies with changes in flare heating. Woods et al. (2004) studied an X17 flare on 28 October 2010 using calibration scans of the Ly α line obtained from the second Solar-Stellar Irradiance Comparison Experiment on board the Solar Radiation and Climate Experiment (SORCE/SOLSTICE; Rottman 2005; Mcclintock, Rottman, and Woods 2005). During this event, the wings of the line were strongly enhanced, by a factor of two, while the line core showed a relatively weaker 20% enhancement. Additionally, a blue asymmetry was observed in the line wings, which the authors did not attribute to a specific mechanism but may have been related to an associated coronal mass ejection. Intriguingly, the blue wing began to enhance prior to the red wing in the flare impulsive phase. It remains unclear whether the observed asymmetry and strong wing enhancement observed during this flare was due to its extreme class, or if similar behaviour is observed in flares of smaller class. To date, comparatively weaker flares have yet to be studied using SORCE/SOLSTICE observations, underscoring the need for such analyses to establish the typical spectral behaviour of Ly α for flares of varying magnitude.

Flaring Ly α spectra observed using the Naval Research Laboratory (NRL) SO82B spectrograph on Skylab's Apollo Telescope Mount (Skylab/ATM; Bartoe et al. 1977) were studied by Canfield and Cook (1978). Their analysis revealed a red enhancement asymmetry in the line wings (between $5 \text{ \AA} < \Delta\lambda_0 < 12 \text{ \AA}$) during a flare; although, this asymmetry was

not statistically significant. Further observations of two additional flares by Skylab/ATM are presented in Canfield and van Hoosier (1980). In one flare, a red asymmetry was seen in the line wings (between $0.5 \text{ \AA} < \Delta\lambda_0 < 1 \text{ \AA}$) during the rise phase, transitioning into a blue asymmetry at flare peak. The second flare exhibited a red asymmetry between the two peaks of the centrally reversed Ly α line core, with the red peak culminating at 30 – 40% brighter than the blue peak. Flaring Ly α line profiles taken by the Laboratoire de Physique Stellaire et Planétaire instrument (LPSP; Bonnet et al. 1978) on the Orbiting Solar Observatory 8 (OSO-8) satellite were presented by Lemaire, Choucq-Bruston, and Vial (1984). These profiles suggest a red asymmetry between the two peaks on either side of the line’s central reversal and a blue asymmetry further out in the line wings. However, the authors provide limited discussion of these features. Brekke et al. (1996) observed an X3 flare using the Upper Atmosphere Research Satellite’s Solar-Stellar Irradiance Comparison Experiment (UARS/SOLSTICE; Rottman, Woods, and Sparn 1993). Their analysis revealed a blue asymmetry in the Ly α line wings, with a 6% integrated enhancement of the line being measured and the largest relative enhancement occurring in the line wings. These studies highlight the diverse spectral variability in the Ly α during different flares. Further study is necessary to understand how variations in underlying flare mechanisms drive the observed changes in Ly α spectral variability.

Although spectrally resolved Ly α flare observations remain scarce, several recent studies have focused on wavelength-integrated observations to study Ly α flare variability. Milligan and Chamberlin (2016) analysed enhancements in the Ly α line during a flare observed with the Extreme Ultraviolet Variability Experiment’s Multi EUV Grating Spectrograph Photometer on the Solar Dynamics Observatory (SDO/EVE MEGS-P; Woods et al. 2012). Their findings revealed good agreement between Ly α and Soft X-ray (SXR) emission. Conversely, a flare observed with SORCE/SOLSTICE exhibited impulsive Ly α emission consistent with the Neupert effect, attributable to differences in instrumental response (Neupert 1968). Expanding on these findings, Milligan et al. (2020) conducted a statistical study of Ly α emission during 477 M- and X-class flares observed with the Extreme Ultraviolet Sensor’s E channel onboard the Geostationary Operational Environmental Satellites (GOES/EUVS-E) during solar cycle 24. For 95% of these flares, Ly α enhancements remained below 10%, with peak emission typically occurring during the impulsive phase. Milligan (2021) further extended the study to include B- and C-class flares observed by GOES/EUVS-E. Average Ly α enhancements were 0.1 – 0.3%, substantially weaker than the 1 – 4% enhancements typically observed during M- and X-class flares. Notably, a C6.6 flare exhibited a 7% enhancement, that was attributed to a failed filament-eruption. Greatorex, Milligan, and Chamberlin (2023) further investigated Ly α variability by comparing Ly α and HXR emission in three flares of equivalent GOES class observed with GOES/EUVS-E and the Reuven Ramaty High Energy Solar Spectroscopic Imager (RHESSI; Lin et al. 2002). Their studies revealed event-dependent variations in Ly α enhancement, with flares that exhibited larger nonthermal electron spectral indices producing greater Ly α enhancements, highlighting the importance of these nonthermal electron properties in understanding Ly α flare variability. These findings have provided significant insights into Ly α flare emission in the absence of spectrally resolved Ly α observations.

This paper presents spectrally-resolved Ly α observations from SORCE/SOLSTICE for two M-class flares. The potential physical mechanisms responsible for flare enhancements across the Ly α line profile are evaluated using a multi-instrument approach. Key observations include HXR count rates from RHESSI, imaging from SDO/AIA, and observations from the Extreme Ultraviolet Imager (EUVI; Wuelser et al. 2004) of the Sun-Earth Connection Coronal and Heliospheric Investigation (SECCHI; Howard et al. 2008), onboard the two Solar TERrestrial RELations Observatory (STEREO; Kaiser et al. 2008) satellites. To validate the SORCE/SOLSTICE Ly α observations, comparisons were made with photometric Ly α observations from GOES/EUVS-E, an established Ly α instrument. Section 2 outlines the instruments used in this study, along with the methodology and analysis applied. The results of this analysis are presented in Section 3. Finally, Section 4 discusses the findings and their implications, along with an overview of the study’s contribution to understanding Ly α flare variability, with insights for future and contemporary Ly α instrumentation.

2. Observations, Methodology & Analysis

This study examines two flares: an M8.3 flare on 12 February 2010 (SOL2010-02-12) in NOAA active region 11046 (N47E16) and an M5.3 flare on 4 July 2012 (SOL2012-07-04) in NOAA active region 11515 (S31W27). The selection of the flares was based on the following criteria:

- Coverage of the impulsive phase by SOLSTICE, RHESSI and GOES/EUVS-E

- Complete or partial imaging coverage at UV wavelengths
- Close proximity to disk-centre to minimise limb-darkening (Milligan et al. 2020; Milligan 2021)

Figure 1 illustrates observations for both events. Panels a.), b.) and c.) display data for SOL2010-02-12. Specifically, panel a.) shows a He II 304 Å image of SOL2010-02-12 from STEREO-A/SECCHI EUVI, panel b.) shows lightcurves from both GOES/EUVS-E and SOLSTICE, and panel c.) shows HXR and SXR lightcurves from RHESSI and the X-ray Sensor on GOES (GOES/XRS). Similarly, panels d.), e.) and f.) depict observations for SOL2012-07-04, with panel d.) featuring an SDO/AIA 1600 Å image, panel e.) presenting lightcurves from SORCE/SOLSTICE, GOES/EUVS-E and SDO/AIA 1600 Å, and panel f.) showing HXR and SXR lightcurves. Lightcurves were generated from Ly α spectra for distinct wavelength ranges within the Ly α line to explore its spectral variability. Comparisons were made between the timings and magnitudes of enhancement in these SORCE/SOLSTICE lightcurves and in photometric observations from GOES/EUVS-E, providing validation of SORCE/SOLSTICE measurements. Further analysis examined the temporal correlation between SORCE/SOLSTICE enhancements and both HXR and SXR enhancements observed by RHESSI and GOES/XRS, respectively. This allowed for the assessment of whether Ly α spectral variability was primarily driven by impulsive or gradual phase processes. To provide additional context, SORCE/SOLSTICE observations were further compared to imaging observations, enabling the separation of chromospheric and coronal contributions to Ly α enhancement.

2.1. SORCE/SOLSTICE

SORCE/SOLSTICE performed disk-integrated wavelength calibration scans through the Ly α line once per orbit from 2003 until 2012, with an effective raster cadence of ~ 1 minute, suitable for the study of spectral behaviour during flares (Woods et al. 2004; Snow et al. 2022). Recently, these data have been made publicly available via the version 18 release of level 3 SORCE/SOLSTICE data products, which are hosted in the SORCE data repository¹. The left and right panels of Figure 2 show SORCE/SOLSTICE Ly α line profiles for SOL2010-02-12 and SOL2012-07-04, respectively.

The wavelength calibration scans consist of rastered spectral irradiance measurements taken between 1203 Å and 1227 Å with a wavelength resolution of 0.35 Å. Each spectral irradiance measurement typically took 1.05 s, and a complete raster of 64 measurements through the entire wavelength range took around 67 s. The duration of a full scan varied but was typically around an hour. A number of these scans coincided with flares, providing some of the only wavelength and flux-calibrated spectrally-resolved observations of Ly α during flares. Further discussion of the SORCE/SOLSTICE wavelength calibration scan observations can be found in Snow et al. (2022). While significant degradation has been observed in other Ly α instruments, such as GOES/EUVS-E and PROBA-2/LYRA, no degradation correction has been applied to these scans (Greatorex, Milligan, and Dammasch 2024). As a result, the irradiance values may contain uncorrected systematic errors. To assess the potential impact of such errors on the timing of flare enhancements, comparisons are made between SORCE/SOLSTICE and GOES/EUVS-E observations.

To probe the behaviour of different parts of the Ly α line during flares, the SORCE/SOLSTICE data were divided into several spectral bands, as defined in Table 1 and illustrated in Figure 2. For each band, data points (in $\text{Wm}^{-2}\text{nm}^{-1}$) were integrated to provide a single irradiance value (in Wm^{-2}) per raster scan. The 1σ combined standard uncertainties provided in the SORCE/SOLSTICE dataset, were propagated to provide the uncertainty in the spectrally-integrated irradiance values.

The Whole Scan band (black shaded bar in Figure 2) includes every data point in each raster, covering both the Ly α and Si III (~ 1206.5 Å) doublet. Also included are the O V line blend at 1218.34 Å in the Ly α near red wing, and the comparatively weaker He II line doublet (~ 1215.1 Å) blended in the Ly α blue wing (CHIANTI² Version 11.0; Dere et al. 1997; Dufresne et al. 2024). The Whole Line band (bright green shaded bar in Figure 2) omits Si III emission and includes data points for only the Ly α line (1209.3 – 1221.9 Å). The remaining bands were defined by specific data points of each raster, rather than fixed wavelength ranges. This was necessary because SORCE/SOLSTICE data points slowly drift in wavelength between raster scans, which can cause data points to enter or exit a given band, leading to discontinuous ‘jumps’ in irradiance. Such effects do not impact the Whole Scan band, as it encompasses all data points, and have minimal impact on the Whole Line band due to the much greater irradiance near the line centroid relative to the band’s edges,

¹<https://lasp.colorado.edu/sorce/data/>

²https://www.chianti-database.org/chianti_linelist.html

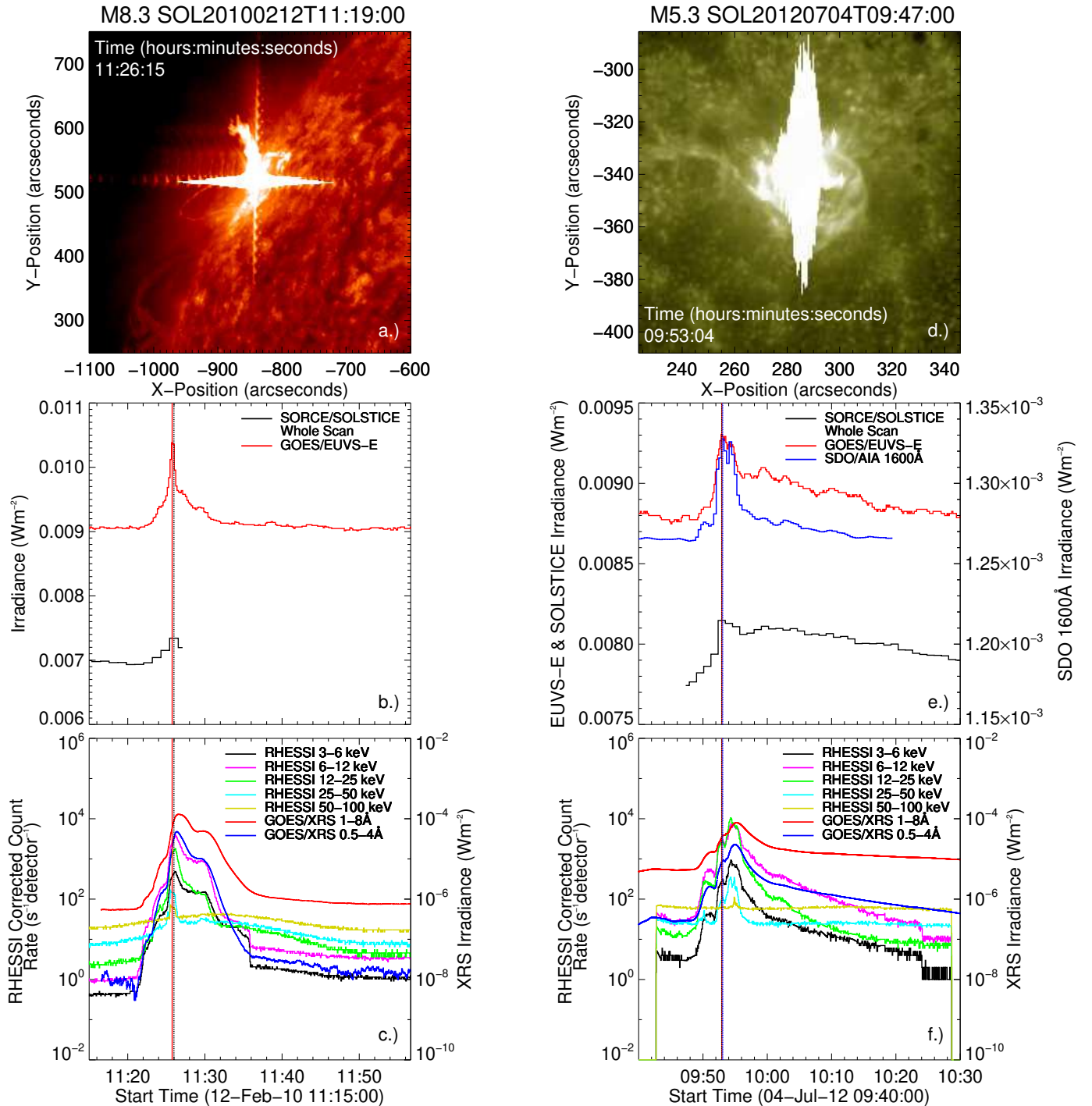


Figure 1. Top panels: Context images from STEREO-A/SECCHI EUVI 304 Å (left) and uncorrected SDO/AIA 1600 Å (right). Middle panels: Integrated Ly α irradiances from SORCE/SOLSTICE and GOES/EUVS-E, with disk-integrated SDO/AIA 1600 Å irradiance for SOL2012-07-04 only. Bottom panels: X-ray corrected count rates and irradiance in different energy channels from RHESSI and GOES/XRS, respectively. Vertical lines indicate peaks in UV emission from lightcurves of the same colour.

making any ‘jumps’ in irradiance negligible. The Line Core band (brown shaded bar in Figure 2) comprises nine data points, with the central point being the closest to the centroid of the Ly α line for a given raster. The Near Wing bands (magenta and cyan shaded bars in Figure 2) contain the nearest six points outside of the Line Core, positioned to the red or blue of the central wavelength. The Far Wings (red and blue shaded bars in Figure 2) include the nearest five points outside of both the Line Core and Near Wings. Finally, the Si III band (orange shaded bar in Figure 2) was defined similarly to the Line Core band, including nine data points centred around the Si III line at 1206 Å.

For SOL2010-02-12, background values for each band were determined by averaging five band integrated measurements before the GOES start time (from 11:14:40 UT to 11:18:09 UT). For SOL2012-07-04, since the SORCE/SOLSTICE scan began slightly after the flare start time, the backgrounds were instead defined as the integrated irradiance measured during the first raster of the SORCE/SOLSTICE observation for each band (09:47:18 UT). This may lead to a slight underestimation of flare enhancements, which were quantified as the percentage increase in irradiance above their respective background value.

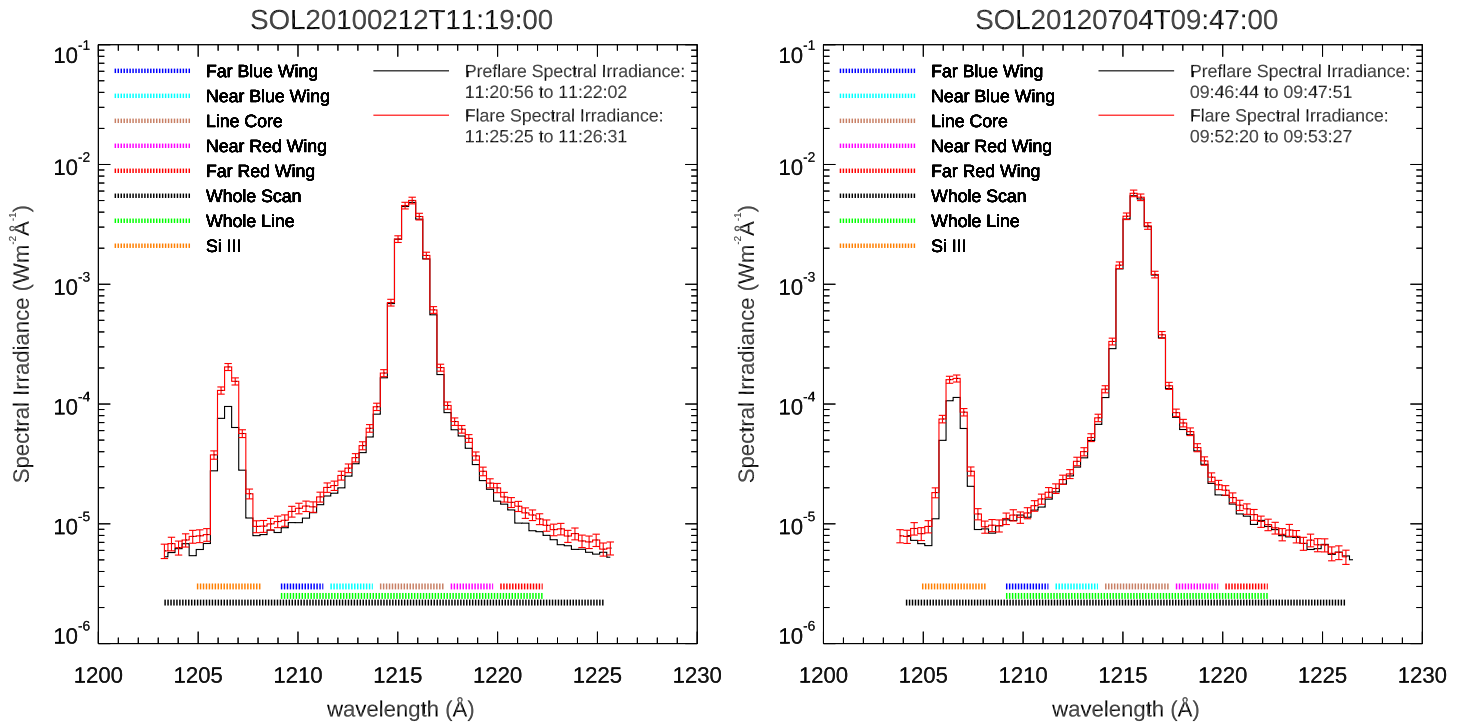


Figure 2. SORCE/SOLSTICE line profiles during SOL2010-02-12 (left) and SOL2012-07-04 (right). For each, a raster scan taken at the time of peak integrated Ly α flare enhancement is plotted as a red line with uncertainty plotted as error bars and a preflare raster is plotted as a black line.

Table 1. Wavelength ranges for the different SORCE/SOLSTICE bands defined for this study.

Band	Wavelength Range (\AA)	Width (\AA)	Δt (s)	Data Points
Whole Scan	1203.0 – 1227.0	24	67	64
Whole Line	1209.3 – 1221.9	12.6	35	~ 36
Si III	~ 1205.0 – 1208.0	3	9.45	9
Line Core	~ 1214.1 – 1217.1	3	9.45	9
Near Red Wing	~ 1217.5 – 1219.5	2	7.35	6
Near Blue Wing	~ 1211.7 – 1213.7	2	7.35	6
Far Red Wing	~ 1219.9 – 1221.9	2	7.35	6
Far Blue Wing	~ 1209.3 – 1211.3	2	7.35	6

The timings and magnitudes of peak flare enhancements were determined for each band, enabling the study of spectral variability in the Ly α line during the two flares. Asymmetry in the Near and Far Wing bands was quantified by calculating the difference in percentage enhancement between the Near Red Wing and Near Blue Wing bands, as well as between the Far Red and Far Blue Wings bands. It should be noted that rastering may introduce instrumentally driven asymmetries, as variation in flare enhancement in the wings may have occurred between the times each wing was scanned.

2.2. GOES/EUVS-E & GOES/XRS

The E channel of EUVS on the GOES-N satellites (GOES/EUVS-E) provided broadband photometry at a cadence of 10.24 s, covering a wavelength range between 1180 \AA and 1270 \AA . This range includes the strong Ly α and Si III lines, as well as several weaker lines. GOES/EUVS-E has been a valuable resource for Ly α observations during flares, with statistical studies of the data made by Milligan et al. (2020) and Milligan (2021). EUVS-E conducted observations between 2006 and 2016, while from 2017 onward, observations have been provided by the B channel of EUVS on GOES-R (GOES/EUVS-B; Eparvier et al. 2009). For SOL2010-02-12, GOES-14 observations were utilised, and for SOL2012-07-04, GOES-15 observations were employed. This leads to potential differences in instrumental performance during each flare. Version 5, level 2 data for both flares was downloaded from the NOAA archive³. These data are scaled to SORCE/SOLSTICE low-cadence observations, providing irradiance calibration, with an additional scaling factor applied to correct instrumental degradation. For each flare, the background was defined as the mean irradiance

³<https://www.ncei.noaa.gov/data/goes-space-environment-monitor>

in a period of 20 minutes before the GOES flare start time, and the standard deviation of irradiance in this period was used to quantify uncertainty. Relative irradiance during each flare was calculated by dividing the measured irradiance by the background value. Flare enhancements and their timings were then determined, allowing for comparison with the timing and magnitude of enhancements measured by SOLSTICE, providing validation. Since the response function of GOES/EUVS-E weights the Ly α and Si III line similarly, comparing GOES/EUVS-E enhancements to those observed in SORCE/SOLSTICE offers insight into the relative significance of each line to the wavelength-integrated flare enhancements measured by GOES/EUVS-E during SOL2010-02-12 and SOL2012-07-04 (Machol, Viereck, and Jones 2014).

The GOES series of satellites also carry the GOES/XRS instrument, which provides broadband observations of X-rays at a cadence of 2 s between 1 – 8 Å and 0.5 – 4 Å via its long and short channels, respectively. Level 2 GOES/XRS data was downloaded from the NOAA archive, and the timings of enhancements in each GOES/XRS channel were compared to Ly α enhancements observed by SOLSTICE. Given that SXR emission characterises the gradual phase of flares, this comparison serves to determine whether Ly α spectral enhancements are driven by gradual phase processes. This analysis is further supported by comparisons to RHESSI observations, which are detailed in Section 2.3.

2.3. RHESSI

During flares, magnetic reconnection drives the acceleration of electrons to high energies (~ 10 – 100 keV). These electrons undergo thick target collisions in the chromosphere, leading to HXR bremsstrahlung emission (Brown 1971; Kontar et al. 2011). RHESSI provided photometrically calibrated spectroscopic and imaging observations of X-rays and γ -rays between 3 keV and 17 MeV, with an energy resolution of ~ 1 – 10 keV, attaining higher resolution at lower energies. To mitigate the effects of detector degradation, RHESSI periodically underwent anneals. Since an anneal was performed closer to the time of SOL2012-07-04, detector sensitivity may have been relatively reduced during SOL2010-02-12. Level 1 RHESSI data for both flares was retrieved from the RHESSI data archive using the observing summary object in SolarSoft. These data include binned X-ray count rates in a number of different channels (including 6 – 12, 25 – 50, 50 – 100 keV) with a cadence of 4 s. Comparisons between enhancements in the HXR 25 – 50 keV and SXR 6 – 12 keV bands with SORCE/SOLSTICE observations provided insights on whether Ly α enhancements were driven by impulsive nonthermal heating or by thermal gradual phase processes.

2.4. STEREO/SECCHI EUVI

The two STEREO/SECCHI EUVI instruments provide full disk imaging of the Sun in four wavelength bands (171 Å, 195 Å, 284 Å, 304 Å) with a cadence between 2.5 and 10 minutes. Together, STEREO-A and STEREO-B provided a stereoscopic view of the Sun. He II 304 Å emission, which is a potential proxy for hydrogen Ly α emission in the quiet Sun (Auchère 2005; Gordino et al. 2022), is extended to the flaring Sun in this study. STEREO/SECCHI EUVI data were downloaded from the Stereo Science Centre and processed to level 1 using SolarSoft’s `secchi_prep` routine. The 304 Å images were visually inspected to determine whether Ly α flare enhancement was likely confined to flare ribbons or if there was a contribution from coronal flare loops. This analysis was performed for SOL2010-02-12, as it occurred prior to the availability of higher resolution, higher cadence imaging from SDO/AIA. These SDO/AIA observations enable a more systematic separation of coronal and chromospheric contributions.

2.5. SDO/AIA

SDO/AIA provides high spatial resolution ($1''$) imaging of the entire solar disk in nine different wavelength bands, with a cadence of 12 s for its extreme ultraviolet (EUV) channels and 24 s for its UV channels. The UV 1600 Å channel, which is dominated by chromospheric emission, was used to provide context imaging for similarly chromospheric Ly α emission during SOL2012-07-04 (Simões et al. 2019). The choice of 1600 Å images over similarly available He II 304 Å images from SDO/AIA was based on the significantly lower saturation observed in the 1600 Å images during the flare, allowing for clearer separation of spatial features. SDO/AIA data was downloaded from the JSOC data archive and processed to level 1.5 using the `aia_prep` routine in SolarSoft. Degradation to the UV channels of SDO/AIA can be corrected using SolarSoft’s `aia_get_response` routine. This correction is applied in the lightcurves seen in panel e.) of Figure 1 but is not applied for the analysis of desaturated images.

To correct for strong saturation in the 1600 Å images, the methods of Kazachenko et al. (2017) were applied. Saturated pixels (> 5000 DN s^{-1}) and pixels within a two-pixel radius

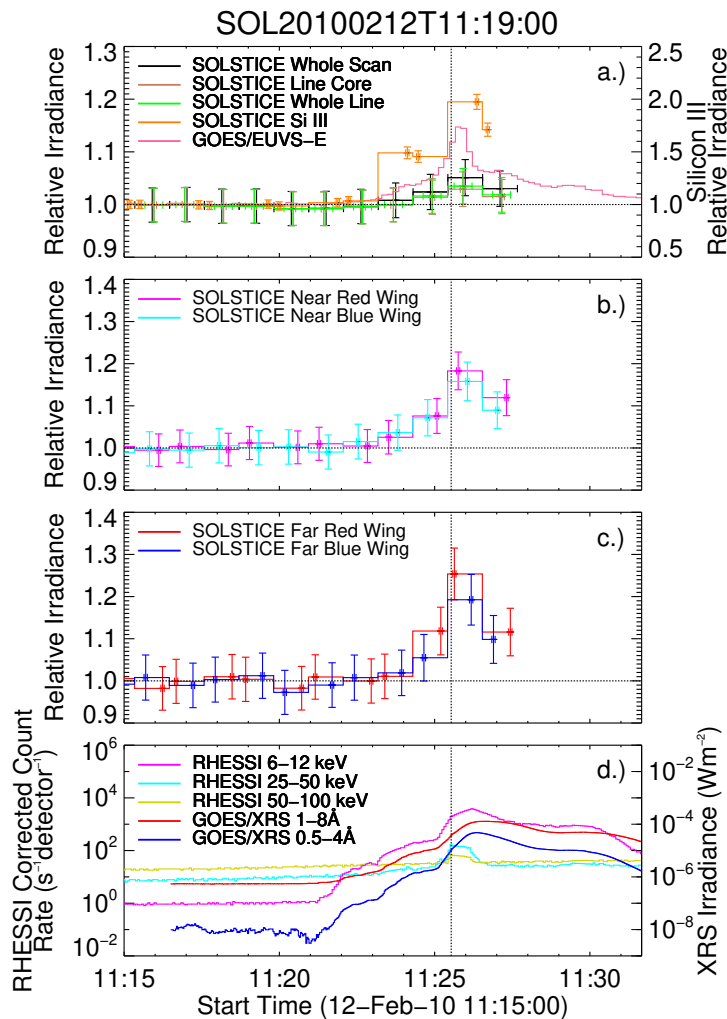


Figure 3. Relative irradiance to the background in each *SORCE/SOLSTICE* band and *GOES/EUVS-E*, with *RHESSI* detector averaged corrected count rates. a.), b.) and c.) show relative enhancements of each *SORCE/SOLSTICE* band during SOL2010-02-12. d.) shows HXR count rates from *RHESSI* in its 6–12 keV, 25–50 keV and 50–100 keV channels along with irradiances from *GOES/XRS* long and short channels. A black dashed line indicates the peak of a HXR burst in the 25–50 keV channel.

in x direction and a 10-pixel radius in y direction from the saturated pixels were selected. The intensity values of these pixels during the saturated period were replaced using values determined from a linear interpolation between the pre-saturated and the post-saturated intensities for the same pixel. Different flare features were identified in the desaturated images by visual inspection, with sections within the images being defined for each feature. The pixel intensities of each section were then summed to generate lightcurves. The timing and magnitude of enhancements in each of these features were then compared to *SORCE/SOLSTICE* spectral Ly α enhancements, offering insight into which features, and hence which physical processes, contributed to the spectral Ly α emission observed during SOL2012-07-04.

3. Results

3.1. SOL2010-02-12T11:19

Figure 3 illustrates the time evolution of relative irradiance in each *SORCE/SOLSTICE* band for SOL2010-02-12, with peak flare enhancements listed in Table 2. During this event, the strongest absolute enhancement in the Ly α line was observed in the Line Core band, reaching $1.91 \times 10^{-4} \text{ Wm}^{-2}$, as seen in panel a.) of Figure 3. While it was strong in absolute terms, this was only a modest relative enhancement. Absolute enhancements the Near Wing bands were over an order of magnitude lower, with the Near Red Wing being enhanced by $1.49 \times 10^{-5} \text{ Wm}^{-2}$ and the Near Blue Wing being enhanced by $1.06 \times 10^{-5} \text{ Wm}^{-2}$. Panel b.) of Figure 3 reveals a 2.5% greater peak relative enhancement in the Near Red Wing compared to the Near Blue Wing, exhibiting a slight red enhancement asymmetry, though this difference falls within uncertainty. The observed asymmetry in the Near Wings

Table 2. Flare enhancements, timings and irradiances along with their uncertainties quoted at 1σ are presented here for GOES/EUVS-E and each SORCE/SOLSTICE band during SOL2010-02-12.

SOL2010-02-12	Peak Relative Flare Enhancement	Peak Irradiance (Wm^{-2})	Peak Excess Irradiance (Wm^{-2})	Median Time (UT)
GOES/EUVS-E	$14.7 \pm 0.3\%$	$10.38 \pm 0.03 \times 10^{-3}$	$1.33 \pm 0.03 \times 10^{-3}$	11:25:45
SORCE/SOLSTICE				
Whole Scan	$5.1 \pm 3.3\%$	$7.34 \pm 0.24 \times 10^{-3}$	$3.56 \pm 2.40 \times 10^{-4}$	11:25:59
Si III	$97.5 \pm 3.6\%$	$2.22 \pm 0.08 \times 10^{-4}$	$1.10 \pm 0.08 \times 10^{-4}$	11:26:21
Whole Line	$3.5 \pm 3.2\%$	$7.07 \pm 0.23 \times 10^{-3}$	$2.38 \pm 2.28 \times 10^{-4}$	11:25:55
Line Core	$2.9 \pm 3.2\%$	$6.76 \pm 0.22 \times 10^{-3}$	$1.91 \pm 2.16 \times 10^{-4}$	11:25:54
Near Red Wing	$18.3 \pm 3.8\%$	$9.61 \pm 0.36 \times 10^{-5}$	$1.49 \pm 3.64 \times 10^{-5}$	11:25:45
Near Blue Wing	$15.8 \pm 4.0\%$	$7.76 \pm 0.31 \times 10^{-5}$	$1.06 \pm 3.07 \times 10^{-5}$	11:26:03
Far Red Wing	$25.4 \pm 4.9\%$	$2.87 \pm 0.14 \times 10^{-5}$	$5.82 \pm 1.41 \times 10^{-6}$	11:25:38
Far Blue Wing	$19.3 \pm 5.0\%$	$2.89 \pm 0.15 \times 10^{-5}$	$4.67 \pm 1.46 \times 10^{-6}$	11:26:11

may also be influenced by the O v (1218.34 Å) line blend. The Far Wing bands had the smallest absolute enhancements in the Ly α line, with the Far Red and Far Blue Wings being enhanced by $5.82 \times 10^{-6} \text{ Wm}^{-2}$ and $4.67 \times 10^{-6} \text{ Wm}^{-2}$, respectively. Panel c.) of Figure 3 shows a red enhancement asymmetry in the Far Wings, with the Far Red Wing exhibiting an enhancement 6.1% greater than the Far Blue Wing, slightly exceeding uncertainty. The Si III line showed strong absolute enhancement of $1.10 \times 10^{-4} \text{ Wm}^{-2}$, with a substantially higher relative enhancement (97.5%) compared to the Ly α bands.

As shown in panels a.), b.) and c.) of Figure 3, the relative enhancement of each Wing band was greater than the Line Core band, consistent with results from Brekke et al. (1996) and Woods et al. (2004). Panel d.) of Figure 3 presents HXR observations from RHESSI in the 6 – 12, 25 – 50 and 50 – 100 keV channels, alongside both channels of GOES/XRS. Good agreement is seen between the timing of a HXR burst and Ly α emission across the line profile. The 25 – 50 keV channel peaked at 11:25:32 UT, aligning with peak enhancements in each SORCE/SOLSTICE band, which all peaked within the same raster (median time 11:25:59 UT). GOES/EUVS-E recorded peak broadband Ly α emission at 11:25:45 UT, closely coinciding with the HXR peak. Of the SORCE/SOLSTICE bands, the peak HXR emission occurred closest in time to the Far Red Wing band, which peaked at 11:25:38 UT. Imaging from STEREO/SECCHI EUVI 304 Å (panel a.) of Figure 1), though heavily saturated, reveals enhancements in both the chromosphere and corona at 11:26:15 UT.

Panel a.) of Figure 3 compares the measured Ly α emission from SORCE/SOLSTICE Whole Scan and GOES/EUVS-E for SOL2010-02-12. GOES/EUVS-E measured peak flare enhancement at 11:25:45 UT, which was within the raster at which SORCE/SOLSTICE Whole Scan had its peak enhancement at 11:25:59 UT. However, the peak relative enhancements were markedly different, with SORCE/SOLSTICE measuring 5.1% and GOES/EUVS-E measuring 14.7%. Panel a.) also illustrates that SORCE/SOLSTICE observed much greater relative flare enhancement of the Si III line at 97.5% than the Ly α Whole Line band at 3.5%. Despite the Ly α line being much stronger than the Si III line in quiescent conditions, the Si III band had a comparable peak excess irradiance of $1.08 \times 10^{-4} \text{ Wm}^{-2}$ to the $2.38 \times 10^{-4} \text{ Wm}^{-2}$ of the Whole Line band for Ly α . This suggests that the Si III line may contribute significantly to the flare excess measured by GOES/EUVS-E as both lines have a similar weighting in the instrument’s response function (Machol, Viereck, and Jones 2014).

3.2. SOL2012-07-04T09:47

The time evolution of relative irradiance in each SORCE/SOLSTICE band for SOL2012-07-04 is shown in Figure 4, with peak flare enhancements listed in Table 3. As with SOL2010-02-12, the Ly α line exhibited its strongest absolute enhancement in the Line Core band during SOL2012-07-04, reaching $3.34 \times 10^{-4} \text{ Wm}^{-2}$. The Near Wing bands showed smaller absolute enhancements, with the Near Red Wing enhancement peaking at $9.38 \times 10^{-6} \text{ Wm}^{-2}$ and the Near Blue Wing enhancement peaking at $5.41 \times 10^{-6} \text{ Wm}^{-2}$. Panel b.) of Figure 4 reveals that the Near Red Wing band’s peak enhancement was 0.8% more than the Near Blue Wing, though this was within uncertainty. The asymmetry may have also been contributed to by the O v line blend. This red enhancement asymmetry in the Near Wing bands later transitioned to blue as the Near Blue Wing peaked, exhibiting a 1.4% greater enhancement than the Near Red wing during the same raster, though this difference also fell within uncertainty.

The Far Wing bands had further diminished absolute enhancements, with the Far Red Wing enhancement peaking at $3.04 \times 10^{-6} \text{ Wm}^{-2}$ and the Far Blue Wing enhancement

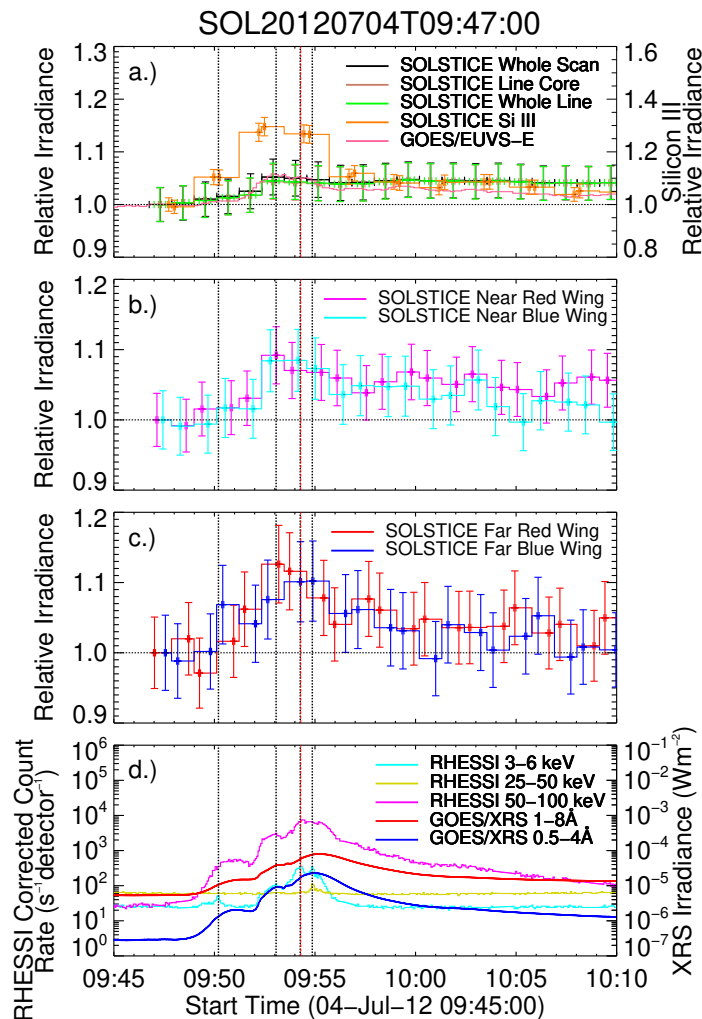


Figure 4. Relative irradiance to the background in each *SORCE/SOLSTICE* band and *GOES/EUVS-E*, with *RHESSI* detector averaged corrected count rates. a.), b.) and c.) show relative enhancements of each *SORCE/SOLSTICE* band during SOL2012-07-04. d.) shows HXR count rates from *RHESSI* in its 6–12 keV, 25–50 keV and 50–100 keV channels along with irradiances from *GOES/XRS* long and short channels. Black dashed lines indicate peaks of HXR bursts in the 25–50 keV channel. The red dashed line indicates a peak in emission from a bright erupting filament seen in *SDO/AIA* 1600 Å images.

peaking at $2.73 \times 10^{-6} \text{ Wm}^{-2}$. As illustrated in panel c.) of Figure 4, the Far Red Wing enhancement exceeded that of the Far Blue Wing by 5.0% at its peak, a difference greater than the uncertainty of the Far Red Wing, but less than that of the Far Blue Wing. Later, this enhancement asymmetry also changed to blue as the Far Blue Wing peaked 2.4% higher than the Far Red Wing during the same raster, though this was within uncertainty.

Table 3. Flare enhancements, timings and irradiances along with their uncertainties quoted at 1σ are presented here for *GOES/EUVS-E* and each *SORCE/SOLSTICE* band during SOL2012-07-04.

SOL2012-07-04	Peak Relative Flare Enhancement	Peak Irradiance (Wm^{-2})	Peak Excess Irradiance (Wm^{-2})	Median Time (UT)
<i>GOES/EUVS-E</i>	$5.8 \pm 0.2\%$	$9.30 \pm 0.02 \times 10^{-3}$	$5.12 \pm 0.16 \times 10^{-4}$	09:52:55
<i>SORCE/SOLSTICE</i>				
Whole Scan	$5.2 \pm 3.2\%$	$8.15 \pm 0.26 \times 10^{-3}$	$4.04 \pm 2.63 \times 10^{-4}$	09:52:55
Si III	$44.4 \pm 3.6\%$	$1.99 \pm 0.07 \times 10^{-4}$	$6.11 \pm 0.72 \times 10^{-5}$	09:52:29
Whole Line	$4.6 \pm 3.2\%$	$7.90 \pm 0.25 \times 10^{-3}$	$3.51 \pm 2.50 \times 10^{-4}$	09:59:39
Line Core	$4.6 \pm 3.1\%$	$7.59 \pm 0.24 \times 10^{-3}$	$3.34 \pm 2.37 \times 10^{-4}$	09:59:39
Near Red Wing	$9.2 \pm 3.7\%$	$1.11 \pm 0.04 \times 10^{-4}$	$9.38 \pm 4.15 \times 10^{-6}$	09:53:04
Near Blue Wing	$8.5 \pm 4.1\%$	$6.92 \pm 0.28 \times 10^{-5}$	$5.41 \pm 2.82 \times 10^{-6}$	09:54:10
Far Red Wing	$12.6 \pm 4.9\%$	$3.04 \pm 0.15 \times 10^{-5}$	$3.40 \pm 1.49 \times 10^{-6}$	09:53:12
Far Blue Wing	$10.2 \pm 5.2\%$	$2.73 \pm 0.14 \times 10^{-5}$	$2.59 \pm 1.45 \times 10^{-6}$	09:54:54

The Whole Scan band peaked earlier than the Whole Line band, likely due to the Si III line exhibiting relatively stronger enhancement in the impulsive phase, while the $\text{Ly}\alpha$ line

was relatively more enhanced during the gradual phase. In panel a.) of Figure 4 it is shown that both the Whole Scan and Whole Line bands exhibit two distinct peaks at 09:52:56 UT and 09:59:39 UT, indicating contributions from both impulsive and gradual phase processes to Ly α enhancement. The Wing bands peaked at distinctly different times: the Near Blue Wing peaking one raster (~ 58 s) after the Near Red Wing and Far Red Wing, while the Far Blue Wing peaked a further raster later. During the raster coinciding with the impulsive peak of the Whole Line band and HXR emission in the RHESSI 25 – 50 keV channel, the Wing bands were more enhanced than the Line Core band, consistent with the findings for SOL2010-02-12 and previous studies (e.g. Brekke et al. 1996; Woods et al. 2004). Panel d.) of Figure 4 displays HXR observations in the 6 – 12, 25 – 50 and 50 – 100 keV channels of RHESSI, alongside both GOES/XRS channels. Four HXR bursts were observed in the 25 – 50 keV channel of RHESSI at 09:50:12 UT, 09:53:04 UT, 09:54:16 UT and 09:54:52 UT. The second HXR burst showed good agreement in time with peaks in Ly α enhancement in the Line Core, Near Red Wing and Far Red Wing band, which occurred during the same raster at 09:52:55 UT, 09:53:04 UT and 09:53:12 UT, respectively. The Near Blue Wing peaked at 09:54:09 UT, close to the third HXR burst, while the Far Blue Wing peaked at 09:54:33 UT, coinciding with the fourth HXR burst.

Panel e.) of Figure 1 shows lightcurves for SORCE/SOLSTICE Whole Scan, GOES/EUVS-E and SDO/AIA 1600 Å during SOL2012-07-04. The timing of flare enhancement was consistent across instruments, with peak enhancements observed in GOES/EUVS-E and SDO/AIA 1600 Å at 09:52:55 UT and 09:53:04 UT, respectively, within the same raster at which SORCE/SOLSTICE Whole Scan peaked at 09:52:55 UT. The SORCE/SOLSTICE Whole Scan recorded a peak enhancement of 5.2%, closely matching the peak GOES/EUVS-E enhancement of 5.8%, as shown in Figure 4. Furthermore, SDO/AIA 1600 Å showed a comparable enhancement of 4.9%. As shown in panel a.) of Figure 4, SORCE/SOLSTICE observed significantly greater relative enhancement of the Si III line of 44.4% compared to the Ly α Whole Line band at 4.6%. The excess irradiance for Si III peaked at $6.11 \times 10^{-5} \text{ Wm}^{-2}$, around one fifth the excess in the Ly α Whole Line band of $3.51 \times 10^{-4} \text{ Wm}^{-2}$. This relative contribution of the Si III line to the Ly α Whole Line excess was smaller during SOL2012-07-04 than SOL2010-02-12.

Figure 5 illustrates the division of SDO/AIA 1600 Å images into filament and flare regions, with corresponding lightcurves shown in Figure 6. The flare region peaked in excess counts at 09:53:30 UT, while the filament region exhibited several distinct peaks at 09:54:18 UT, 09:59:30 UT, 10:03:30 UT and 10:10:18 UT, displayed in panels a.), b.), c.) and d.) of Figure 5, respectively. The first filament peak coincided with peak enhancements in the Near and Far Blue Wing bands of SORCE/SOLSTICE at 09:54:10 UT and 09:54:54 UT, respectively, suggesting that blue-shifted emission from the erupting filament contributed to these enhancements. The subsequent filament peaks correlated with the timing of gradual phase enhancements observed by GOES/EUVS-E at 09:59:06 UT, 10:02:33 UT and 10:09:39 UT, as shown in Figure 6, suggesting that the bright erupting filament also contributed to the gradual phase Ly α enhancements. Similar findings of filament contributions to gradual phase Ly α enhancement were reported by Wauters et al. (2022) during an M6.7 flare using SDO/AIA 1600 Å and PROBA-2/LYRA observations.

3.3. Comparison Between Flares

The comparison of SOL2010-02-12 and SOL2012-07-04 (Figures 3 and 4) provides valuable insights into the mechanisms driving Ly α spectral variability during flares. Both events exhibited similar peak enhancements of the Whole Scan band, with values of 5.1% for SOL2010-02-12 and 5.2% for SOL2012-07-04. However, GOES/EUVS-E observed a significantly higher peak enhancement of 14.7% during SOL2010-02-12, compared to the 5.8% enhancement observed during SOL2012-07-04. Near Wing enhancements were significantly greater during SOL2010-02-12, with peak values of 18.3% and 15.8% in the Near Red and Near Blue, respectively, compared to enhancements of 9.2% and 8.5% for SOL2012-07-04. A similar trend was seen in the Far Wing bands, with SOL2010-02-12 exhibiting larger enhancements during of 25.4% and 19.3% for the Far Red and Far Blue bands, respectively, compared to 12.6% and 10.2% during SOL2012-07-04. The Si III line also showed significantly greater peak enhancement of 97.5% during SOL2010-02-12, in contrast to the 44.4% for SOL2012-07-04. For both events, enhancements in each SORCE/SOLSTICE band were temporally correlated with bursts of HXR emission, indicating these enhancements were likely driven by nonthermal processes. Additionally, enhancements in the Near and Far Blue bands of SOLSTICE, as well as in GOES/EUVS-E during SOL2012-07-04, were attributed to a bright filament-eruption observed by SDO/AIA. Blue wing enhancements associated with filament eruptions during flares have also been identified in sun-as-a-star observations from SDO/EVE, in various other chromospheric and transition region lines such as Ly β , He I 584.3 Å and O V 629.7 Å (Brown, Fletcher, and Labrosse 2016; Xu et al. 2022; Lu

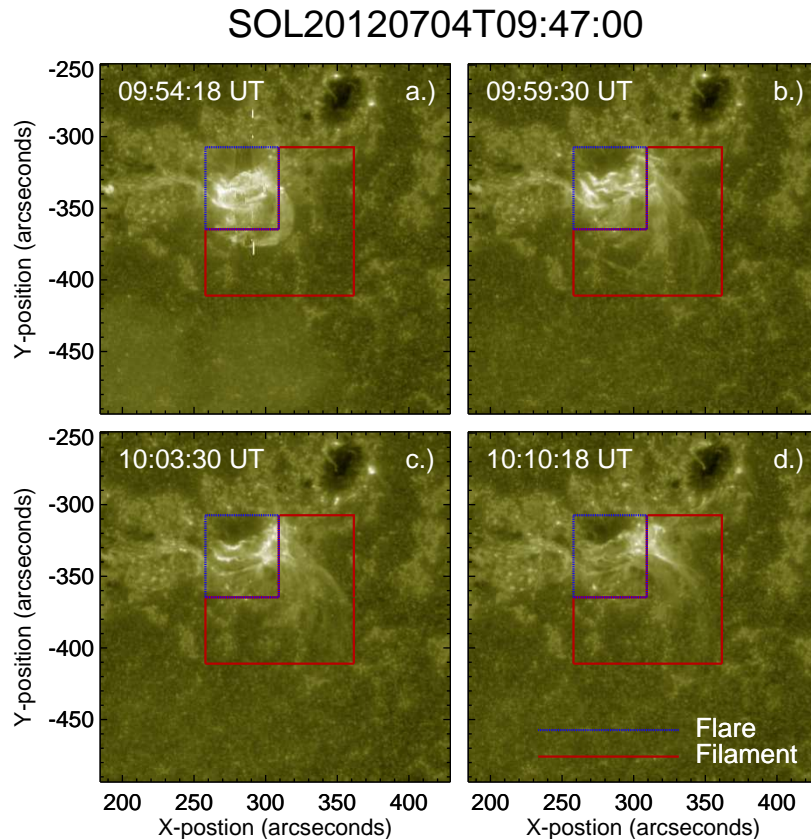


Figure 5. Desaturated SDO/AIA 1600 Å images of SOL2012-07-04. The flaring region is contained in the blue box while the region of filament-eruption is contained in the red box. Images shown are at times at which peaks in filament-eruption emission are seen.

et al. 2023; Otsu and Asai 2024). Although STEREO/SECCHI EUVI images revealed a filament-eruption during SOL2010-02-12, it was not possible to compare its emission to that in Ly α due to significant saturation and the low cadence of the observations. As both events had similar GOES class, it is likely that varied contributions of flare processes such as nonthermal heating, conduction and radiative cooling between the flares drove the observed differences in Ly α variability.

4. Discussion & Conclusions

This study analysed the spectral irradiance variability of Ly α emission during two M-class flares, SOL2010-02-12 and SOL2012-07-04, using newly-released high-cadence calibration scans from SORCE/SOLSTICE. By comparing Ly α spectral enhancements with HXR and UV observations, the heating mechanisms responsible for the observed variability were investigated. During SOL2010-02-12, good agreement was observed between HXR emission and enhancements across the Ly α line profile, suggesting that nonthermal heating primarily drove these Ly α enhancements. Additionally, during SOL2012-07-04, enhancements in the Line Core and Red Wing bands cotemporal with a HXR burst further supported a nonthermal origin for the spectral variability. These findings are consistent with previous studies that compared HXR emission and enhancement of other chromospheric lines such as H α (Kurokawa, Takakura, and Ohki 1988; Radziszewski, Rudawy, and Phillips 2011), supporting the role of nonthermal electrons in driving chromospheric Ly α enhancement during flares. The Blue Wing bands during SOL2012-07-04 exhibited peak enhancements at a later time, coincident with a further HXR burst and emission from a bright filament-eruption seen in SDO/AIA 1600 Å images. This overlap makes it unclear whether the Blue Wing enhancements were primarily driven by nonthermal chromospheric heating or by filament-related emission. Furthermore, gradual phase filament emission correlated with Ly α enhancements observed by GOES/EUVS-E, supporting findings from previous studies (Milligan 2021; Wauters et al. 2022). These results provide further evidence that filament-eruptions likely contribute to Ly α flare variability along with traditional flare processes such as nonthermal heating, conduction and radiative cooling.

Both flares exhibited red asymmetry in wing enhancements, likely indicative of chromospheric evaporation (Hong et al. 2019). During SOL2012-07-04, the red enhancement asymmetry changed to blue, coinciding with emission from a filament eruption. This suggests

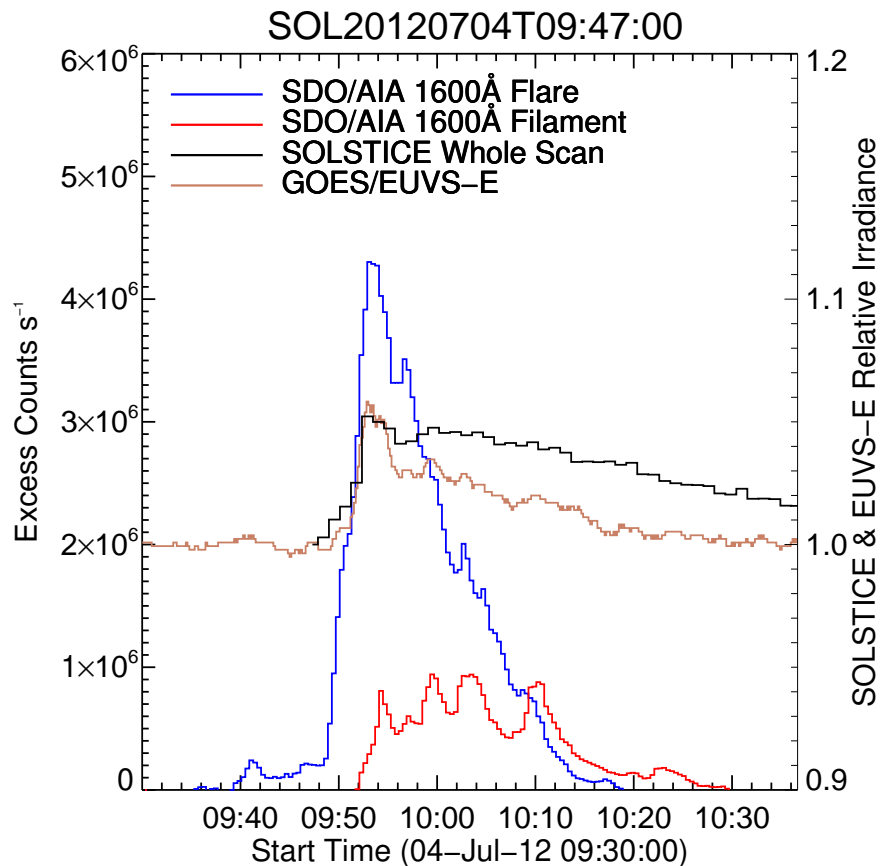


Figure 6. Lightcurves of SDO/AIA 1600 Å excess counts for SOL2012-07-04 flare (blue) and filament (red) regions. Ly α relative irradiance is also shown for GOES/EUVS-E and SORCE/SOLSTICE Whole Scan band in brown and black, respectively.

the filament may have contributed to the observed blue asymmetry via blue-shifted emission. While previous observational and theoretical studies have mostly focused on Ly α emission driven by heating of the chromosphere by nonthermal particles and thermal conduction, future research should also explore the potential impact of emission from filament eruptions on spectral variability during flares.

Comparisons between GOES/EUVS-E and SORCE/SOLSTICE revealed marked differences in Ly α enhancement during SOL2010-02-12, while better agreement was found between the instruments during SOL2012-07-04. These discrepancies highlight ongoing challenges in Ly α flare observations, with different instruments providing disparate results for the same events (e.g. Milligan and Chamberlin 2016; Greatorex, Milligan, and Dammasch 2024). Future comparisons of SORCE/SOLSTICE observations with other Ly α instruments may help uncover the reasons for these disparities.

The key conclusion from this study is that Ly α spectral variability during flares is likely primarily driven by nonthermal processes in the chromosphere but may also be influenced by coronal structures, such as filament-eruptions. Comparisons between SORCE/SOLSTICE observations and simulated Ly α flare line profiles may further constrain the results of the simulations, providing further insight on the mechanisms driving Ly α spectral variability (Brown et al. 2018; Kerr et al. 2023). Additionally, SORCE/SOLSTICE observations may provide insight into Ly α variability during stellar flares and the influence of flaring Ly α on exoplanet atmospheres (Lecavelier des Etangs et al. 2012; Hazra et al. 2022).

Despite its contributions, this study faced several limitations. The small number of SORCE/SOLSTICE flare observations restricted the statistical scope of this analysis, with only two flares being studied. Additionally, the rastering nature of SOLSTICE, combined with its modest wavelength resolution (0.35 Å) and substantial irradiance uncertainty hampered the interpretation of Ly α spectral variability. As a result, the analysed flares, which had uncharacteristically large Ly α enhancements, may not reflect the spectral variability of weaker flares.

Upcoming instruments, such as the EUV High-Throughput Spectroscopic Telescope aboard the SOLAR-C mission (EUVST; Watanabe 2014; Shimizu et al. 2019), are expected to provide state-of-the-art, spectrally resolved Ly α flare observations. EUVST will feature a dramatically higher wavelength resolution (0.008 Å) and cadence (1 s) than SOLSTICE. This will eliminate any asymmetries caused by rastering and enable a more precise interpretation of the flare dynamics driving spectral variability by resolving spatial features in the chromosphere and corona. Additionally, the Solar eruptionN Integral Field Spectrograph

(SNIFS) will provide high wavelength resolution (0.0033 \AA) and cadence (1 s) observations of Ly α , potentially capturing a flare during its sounding rocket flight. These instruments should combine to provide a wealth of high-quality flare observations, enabling the detection of smaller Ly α enhancements than previously possible. This will facilitate both statistical and qualitative studies, offering further insights into flare dynamics in the chromosphere and corona.

Combined Ly α spectral and HXR observations from EUVST, SNIFS, Solar Orbiter's Spectrometer Telescope for Imaging X-rays (SolO/STIX; Müller et al. 2020; Krucker et al. 2020), and the Hard X-ray Imager aboard the Advanced Space-Based Solar Observatory (ASO-S/HXI; Zhang et al. 2019) will enable a more conclusive determination of the relationship between Ly α spectral variability and the properties of nonthermal electrons that drive this variability. These observations will benefit from true Ly α imaging from EUVST, SNIFS, SolO/EUI and Lyman Solar Telescope onboard ASO-S (ASO-S/LST Gan et al. 2019; Li et al. 2019). The combination of spectral and imaging data will enable the disentanglement of chromospheric and coronal contributions to Ly α spectral variability. Furthermore, HXR observations will enable the comparison of spatial sources of Ly α and HXR emission, revealing whether Ly α emission in different features is driven by nonthermal heating. This analysis will provide a deeper understanding of the physical processes driving Ly α spectral variability during flares.

Acknowledgements L.H.M. acknowledges support from the Department for the Economy (DfE) Northern Ireland postgraduate studentship scheme. R.O.M. and E.C.B. acknowledge support from STFC grants ST/W001144/1 and ST/X000923/1.

References

- Auchère, F.: 2005, Effect of the H I Ly α Chromospheric Flux Anisotropy on the Total Intensity of the Resonantly Scattered Coronal Radiation. *Astrophys. J.* **622**, 737. DOI. ADS.
- Bartoe, J.-D.F., Brueckner, G.E., Purcell, J.D., Tousey, R.: 1977, Extreme ultraviolet spectrograph ATM experiment S082B. *Applied Optics* **16**, 879. DOI. ADS.
- Bonnet, R.M., Lemaire, P., Vial, J.C., Artzner, G., Gouttebroze, P., Jouchoux, A., Leibacher, J.W., Skumanich, A., Vidal-Madjar, A.: 1978, The LPSP instrument on OSO 8. II. In-flight performance and preliminary results. *Astrophys. J.* **221**, 1032. DOI. ADS.
- Brekke, P., Rottman, G.J., Fontenla, J., Judge, P.G.: 1996, The Ultraviolet Spectrum of a 3B Class Flare Observed with SOLSTICE. *Astrophys. J.* **468**, 418. DOI. ADS.
- Brown, J.C.: 1971, The Deduction of Energy Spectra of Non-Thermal Electrons in Flares from the Observed Dynamic Spectra of Hard X-Ray Bursts. *Sol. Phys.* **18**, 489. DOI. ADS.
- Brown, S.A., Fletcher, L., Labrosse, N.: 2016, Doppler speeds of the hydrogen Lyman lines in solar flares from EVE. *Astron. Astrophys.* **596**, A51. DOI. ADS.
- Brown, S.A., Fletcher, L., Kerr, G.S., Labrosse, N., Kowalski, A.F., De La Cruz Rodríguez, J.: 2018, Modeling of the Hydrogen Lyman Lines in Solar Flares. *Astrophys. J.* **862**, 59. DOI. ADS.
- Canfield, R.C., Cook, J.W.: 1978, ATM evidence for a nonthermal proton/electron energy flux ratio in solar flares. *Astrophys. J.* **225**, 650. DOI. ADS.
- Canfield, R.C., van Hoosier, M.E.: 1980, Observed Ly α profiles for two solar flares: 14:12 UT 15 June, 1973 and 23:16 UT 21 January, 1974. *Sol. Phys.* **67**, 339. DOI. ADS.
- Dere, K.P., Landi, E., Mason, H.E., Monsignori Fossi, B.C., Young, P.R.: 1997, CHIANTI - an atomic database for emission lines. *Astron. Astrophys. Suppl.* **125**, 149. DOI. ADS.
- Dominique, M., Hochedez, J.-F., Schmutz, W., Dammasch, I.E., Shapiro, A.I., Kretzschmar, M., Zhukov, A.N., Gillotay, D., Stockman, Y., BenMoussa, A.: 2013, The LYRA Instrument Onboard PROBA2: Description and In-Flight Performance. *Sol. Phys.* **286**, 21. DOI. ADS.
- Dufresne, R.P., Del Zanna, G., Young, P.R., Dere, K.P., Deliporanidou, E., Barnes, W.T., Landi, E.: 2024, CHIANTI—An Atomic Database for Emission Lines—Paper. XVIII. Version 11, Advanced Ionization Equilibrium Models: Density and Charge Transfer Effects. *Astrophys. J.* **974**, 71. DOI. ADS.
- Eparvier, F.G., Crotser, D., Jones, A.R., McClintock, W.E., Snow, M., Woods, T.N.: 2009, The Extreme Ultraviolet Sensor (EUVS) for GOES-R. In: Fineschi, S., Fennelly, J.A. (eds.) *Solar Physics and Space Weather Instrumentation III, Society of Photo-Optical Instrumentation Engineers (SPIE) Conference Series* **7438**, 743804. DOI. ADS.
- Fontenla, J.M., Avrett, E.H., Loeser, R.: 1991, Energy Balance in the Solar Transition Region. II. Effects of Pressure and Energy Input on Hydrostatic Models. *Astrophys. J.* **377**, 712. DOI. ADS.
- Gan, W.-Q., Zhu, C., Deng, Y.-Y., Li, H., Su, Y., Zhang, H.-Y., Chen, B., Zhang, Z., Wu, J., Deng, L., Huang, Y., Yang, J.-F., Cui, J.-J., Chang, J., Wang, C., Wu, J., Yin, Z.-S., Chen, W., Fang, C., Yan, Y.-H., Lin, J., Xiong, W.-M., Chen, B., Bao, H.-C., Cao, C.-X., Bai, Y.-P., Wang, T., Chen, B.-L., Li, X.-Y., Zhang, Y., Feng, L., Su, J.-T., Li, Y., Chen, W., Li, Y.-P., Su, Y.-N., Wu, H.-Y., Gu, M., Huang, L., Tang, X.-J.: 2019, Advanced Space-based Solar Observatory (ASO-S): an overview. *Research in Astronomy and Astrophysics* **19**, 156. DOI. ADS.
- Gordino, M., Auchère, F., Vial, J.-C., Bocchialini, K., Hassler, D.M., Bando, T., Ishikawa, R., Kano, R., Kobayashi, K., Narukage, N., Trujillo Bueno, J., Winebarger, A.: 2022, Empirical relations between the intensities of Lyman lines of H and He⁺. *Astron. Astrophys.* **657**, A86. DOI. ADS.
- Greatorex, H.J., Milligan, R.O., Chamberlin, P.C.: 2023, Observational Analysis of Ly α Emission in Equivalent-magnitude Solar Flares. *Astrophys. J.* **954**, 120. DOI. ADS.
- Greatorex, H.J., Milligan, R.O., Dammasch, I.E.: 2024, On the Instrumental Discrepancies in Lyman-alpha Observations of Solar Flares. *arXiv e-prints*, arXiv:2411.00736. ADS.
- Handy, B.N., Tarbell, T.D., Wolfson, C.J., Korendyke, C.M., Vourlidas, A.: 1999, Calibrated H I Lyman α Observations with TRACE. *Sol. Phys.* **190**, 351. DOI. ADS.
- Hazra, G., Vidotto, A.A., Carolan, S., Villarreal D'Angelo, C., Manchester, W.: 2022, The impact of coronal mass ejections and flares on the atmosphere of the hot Jupiter HD189733b. *Mon. Not. R. Astron. Soc.* **509**, 5858. DOI. ADS.

- Hong, J., Li, Y., Ding, M.D., Carlsson, M.: 2019, The Response of the Ly α Line in Different Flare Heating Models. *Astrophys. J.* **879**, 128. DOI. ADS.
- Howard, R.A., Moses, J.D., Vourlidas, A., Newmark, J.S., Socker, D.G., Plunkett, S.P., Korendyke, C.M., Cook, J.W., Hurley, A., Davila, J.M., Thompson, W.T., St Cyr, O.C., Mentzell, E., Mehalick, K., Lemen, J.R., Wuelsel, J.P., Duncan, D.W., Tarbell, T.D., Wolfson, C.J., Moore, A., Harrison, R.A., Waltham, N.R., Lang, J., Davis, C.J., Eyles, C.J., Mapson-Menard, H., Simnett, G.M., Halain, J.P., Defise, J.M., Mazy, E., Rochus, P., Mercier, R., Ravet, M.F., Delmotte, F., Auchere, F., Delaboudiniere, J.P., Bothmer, V., Deutsch, W., Wang, D., Rich, N., Cooper, S., Stephens, V., Maahs, G., Baugh, R., McMullin, D., Carter, T.: 2008, Sun Earth Connection Coronal and Heliospheric Investigation (SECCHI). *Space Sci. Rev.* **136**, 67. DOI. ADS.
- Kaiser, M.L., Kucera, T.A., Davila, J.M., St. Cyr, O.C., Guhathakurta, M., Christian, E.: 2008, The STEREO Mission: An Introduction. *Space Sci. Rev.* **136**, 5. DOI. ADS.
- Kazachenko, M.D., Lynch, B.J., Welsch, B.T., Sun, X.: 2017, A Database of Flare Ribbon Properties from the Solar Dynamics Observatory. I. Reconnection Flux. *Astrophys. J.* **845**, 49. DOI. ADS.
- Kerr, G.S., Allred, J.C., Kowalski, A.F., Milligan, R.O., Hudson, H.S., Zambrana Prado, N., Kucera, T.A., Brosius, J.W.: 2023, Prospects of Detecting Nonthermal Protons in Solar Flares via Lyman Line Spectroscopy: Revisiting the Orrall-Zirker Effect. *Astrophys. J.* **945**, 118. DOI. ADS.
- Kontar, E.P., Brown, J.C., Emslie, A.G., Hajdas, W., Holman, G.D., Hurford, G.J., Kašparová, J., Mallik, P.C.V., Massone, A.M., McConnell, M.L., Piana, M., Prato, M., Schmahl, E.J., Suarez-Garcia, E.: 2011, Deducing Electron Properties from Hard X-ray Observations. *Space Sci. Rev.* **159**, 301. DOI. ADS.
- Krucker, S., Hurford, G.J., Grimm, O., Kögl, S., Gröbelbauer, H.-P., Etesi, L., Casadei, D., Csillaghy, A., Benz, A.O., Arnold, N.G., Molendini, F., Orleaniski, P., Schori, D., Xiao, H., Kuhar, M., Hochmuth, N., Felix, S., Schramka, F., Marcin, S., Kobler, S., Iseli, L., Dreier, M., Wiehl, H.J., Kleint, L., Battaglia, M., Lastufka, E., Sathiapal, H., Lapadula, K., Bednarzik, M., Birrer, G., Stutz, S., Wild, C., Marone, F., Skup, K.R., Cichocki, A., Ber, K., Rutkowski, K., Bujwan, W., Juchnikowski, G., Winkler, M., Darmetko, M., Michalska, M., Seweryn, K., Białek, A., Osica, P., Sylwester, J., Kowalinski, M., Ścisłowski, D., Siarkowski, M., Stęślicki, M., Mrozek, T., Podgórski, P., Meuris, A., Limousin, O., Gevin, O., Le Mer, I., Brun, S., Strugarek, A., Vilmer, N., Musset, S., Maksimović, M., Fárník, F., Kozáček, Z., Kašparová, J., Mann, G., Önel, H., Warmuth, A., Rendtel, J., Anderson, J., Bauer, S., Dionies, F., Paschke, J., Plüschke, D., Woche, M., Schuller, F., Veronig, A.M., Dickson, E.C.M., Gallagher, P.T., Maloney, S.A., Bloomfield, D.S., Piana, M., Massone, A.M., Benvenuto, F., Massa, P., Schwartz, R.A., Dennis, B.R., van Beek, H.F., Rodríguez-Pacheco, J., Lin, R.P.: 2020, The Spectrometer/Telescope for Imaging X-rays (STIX). *Astron. Astrophys.* **642**, A15. DOI. ADS.
- Kurokawa, H., Takakura, T., Ohki, K.: 1988, Close relationship between H-alpha and hard X-ray emissions at the impulsive phase of a solar flare. *Publ. Astron. Soc. Japan* **40**, 357. ADS.
- Lecavelier des Etangs, A., Bourrier, V., Wheatley, P.J., Dupuy, H., Ehrenreich, D., Vidal-Madjar, A., Hébrard, G., Ballester, G.E., Désert, J.-M., Ferlet, R., Sing, D.K.: 2012, Temporal variations in the evaporating atmosphere of the exoplanet HD 189733b. *Astron. Astrophys.* **543**, L4. DOI. ADS.
- Lemaire, P., Choucq-Bruston, M., Vial, J.-C.: 1984, Simultaneous H and K Ca ii, h and k Mg ii, L α and L β H i profiles of the April 15, 1978 solar flare observed with the OSO-8/L.P.S.P. experiment. *Sol. Phys.* **90**, 63. DOI. ADS.
- Lemen, J.R., Title, A.M., Akin, D.J., Boerner, P.F., Chou, C., Drake, J.F., Duncan, D.W., Edwards, C.G., Friedlaender, F.M., Heyman, G.F., Hurlburt, N.E., Katz, N.L., Kushner, G.D., Levay, M., Lindgren, R.W., Mathur, D.P., McFeaters, E.L., Mitchell, S., Rehse, R.A., Schrijver, C.J., Springer, L.A., Stern, R.A., Tarbell, T.D., Wuelsel, J.-P., Wolfson, C.J., Yanari, C., Bookbinder, J.A., Cheimets, P.N., Caldwell, D., Deluca, E.E., Gates, R., Golub, L., Park, S., Podgorski, W.A., Bush, R.I., Scherrer, P.H., Gummin, M.A., Smith, P., Auken, G., Jerram, P., Pool, P., Souffi, R., Windt, D.L., Beardsley, S., Clapp, M., Lang, J., Waltham, N.: 2012, The Atmospheric Imaging Assembly (AIA) on the Solar Dynamics Observatory (SDO). *Sol. Phys.* **275**, 17. DOI. ADS.
- Li, H., Chen, B., Feng, L., Li, Y., Huang, Y., Li, J.-W., Lu, L., Xue, J.-C., Ying, B.-L., Zhao, J., Yang, Y.-T., Gan, W.-Q., Fang, C., Song, K.-F., Wang, H., Guo, Q.-F., He, L.-P., Zhu, B., Zhu, C., Deng, L., Bao, H.-C., Cao, C.-X., Yang, Z.-G.: 2019, The Lyman-alpha Solar Telescope (LST) for the ASO-S mission — I. Scientific objectives and overview. *Research in Astronomy and Astrophysics* **19**, 158. DOI. ADS.
- Li, Y., Li, Q., Song, D.-C., Battaglia, A.F., Xiao, H., Krucker, S., Schühle, U., Li, H., Gan, W., Ding, M.D.: 2022, The Ly α Emission in a C1.4 Solar Flare Observed by the Extreme Ultraviolet Imager aboard Solar Orbiter. *Astrophys. J.* **936**, 142. DOI. ADS.
- Lin, R.P., Dennis, B.R., Hurford, G.J., Smith, D.M., Zehnder, A., Harvey, P.R., Curtis, D.W., Pankow, D., Turin, P., Bester, M., Csillaghy, A., Lewis, M., Madden, N., van Beek, H.F., Appleby, M., Raudorf, T., McTiernan, J., Ramaty, R., Schmahl, E., Schwartz, R., Krucker, S., Abiad, R., Quinn, T., Berg, P., Hashii, M., Sterling, R., Jackson, R., Pratt, R., Campbell, R.D., Malone, D., Landis, D., Barrington-Leigh, C.P., Slassi-Sennou, S., Cork, C., Clark, D., Amato, D., Orwig, L., Boyle, R., Banks, I.S., Shirey, K., Tolbert, A.K., Zarro, D., Snow, F., Thomsen, K., Henneck, R., Mchedlishvili, A., Ming, P., Fivian, M., Jordan, J., Wanner, R., Crubb, J., Preble, J., Matranga, M., Benz, A., Hudson, H., Canfield, R.C., Holman, G.D., Crannell, C., Kosugi, T., Emslie, A.G., Vilmer, N., Brown, J.C., Johns-Krull, C., Aschwanden, M., Metcalf, T., Conway, A.: 2002, The Reuven Ramaty High-Energy Solar Spectroscopic Imager (RHessi). *Sol. Phys.* **210**, 3. DOI. ADS.
- Lu, H.-p., Tian, H., Chen, H.-c., Xu, Y., Hou, Z.-y., Bai, X.-y., Tan, G.-y., Yang, Z.-h., Ren, J.: 2023, Full Velocities and Propagation Directions of Coronal Mass Ejections Inferred from Simultaneous Full-disk Imaging and Sun-as-a-star Spectroscopic Observations. *Astrophys. J.* **953**, 68. DOI. ADS.
- Machol, J., Viereck, R., Jones, A.: 2014, GOES NOP EUV Data, v2. Technical report, National Oceanic and Atmospheric Association. https://www.ngdc.noaa.gov/stp/GOES/doc/GOES_NOP_EUV_v2.pdf.
- McClintock, W.E., Rottman, G.J., Woods, T.N.: 2005, Solar-Stellar Irradiance Comparison Experiment II (Solstice II): Instrument Concept and Design. *Sol. Phys.* **230**, 225. DOI. ADS.
- Milligan, R.O.: 2021, Solar Irradiance Variability Due to Solar Flares Observed in Lyman-Alpha Emission. *Sol. Phys.* **296**, 51. DOI. ADS.
- Milligan, R.O., Chamberlin, P.C.: 2016, Anomalous temporal behaviour of broadband Ly α observations during solar flares from SDO/EVE. *Astron. Astrophys.* **587**, A123. DOI. ADS.
- Milligan, R.O., Hudson, H.S., Chamberlin, P.C., Hannah, I.G., Hayes, L.A.: 2020, Lyman-alpha Variability During Solar Flares Over Solar Cycle 24 Using GOES-15/EUVS-E. *Space Weather* **18**, e02331. DOI. ADS.
- Müller, D., St. Cyr, O.C., Zouganelis, I., Gilbert, H.R., Marsden, R., Nieves-Chinchilla, T., Antonucci, E., Auchère, F., Berghmans, D., Horbury, T.S., Howard, R.A., Krucker, S., Maksimovic, M., Owen, C.J., Rochus, P., Rodríguez-Pacheco, J., Romoli, M., Solanki, S.K., Bruno, R., Carlsson, M., Fludra, A., Harra, L., Hassler, D.M., Livi, S., Louarn, P., Peter, H., Schühle, U., Teriaca, L., del Toro Iniesta, J.C., Wimmer-Schweingruber, R.F., Marsch, E., Velli, M., De Groof, A., Walsh, A., Williams, D.: 2020, The Solar Orbiter mission. Science overview. *Astron. Astrophys.* **642**, A1. DOI. ADS.

- Neupert, W.M.: 1968, Comparison of Solar X-Ray Line Emission with Microwave Emission during Flares. *Astrophys. J. Lett.* **153**, L59. DOI ADS.
- Otsu, T., Asai, A.: 2024, Multiwavelength Sun-as-a-star Analysis of the M8.7 Flare on 2022 October 2 Using H α and EUV Spectra Taken by SMART/SDDI and SDO/EVE. *Astrophys. J.* **964**, 75. DOI ADS.
- Pesnell, W.D., Thompson, B.J., Chamberlin, P.C.: 2012, The Solar Dynamics Observatory (SDO). *Sol. Phys.* **275**, 3. DOI ADS.
- Radziszewski, K., Rudawy, P., Phillips, K.J.H.: 2011, High time resolution observations of solar H α flares. II. Search for signatures of electron beam heating. *Astron. Astrophys.* **535**, A123. DOI ADS.
- Rochus, P., Auchère, F., Berghmans, D., Harra, L., Schmutz, W., Schühle, U., Addison, P., Appourchaux, T., Aznar Cuadrado, R., Baker, D., Barbay, J., Bates, D., BenMoussa, A., Bergmann, M., Beurthe, C., Borgo, B., Bonte, K., Bouzit, M., Bradley, L., Büchel, V., Buchlin, E., Büchner, J., Cabé, F., Cadiergues, L., Chaigneau, M., Chares, B., Choque Cortez, C., Coker, P., Condamin, M., Coumar, S., Curdt, W., Cutler, J., Davies, D., Davison, G., Defise, J.-M., Del Zanna, G., Delmotte, F., Delouille, V., Dolla, L., Dumesnil, C., Dürig, F., Enge, R., François, S., Fourmond, J.-J., Gillis, J.-M., Giordanengo, B., Gissot, S., Green, L.M., Guerreiro, N., Guilbaud, A., Gyo, M., Haberreiter, M., Hafiz, A., Hailey, M., Halain, J.-P., Hansotte, J., Hecquet, C., Heerlein, K., Hellin, M.-L., Hemsley, S., Hermans, A., Hervier, V., Hochedez, J.-F., Houbrechts, Y., Ihsan, K., Jacques, L., Jérôme, A., Jones, J., Kahle, M., Kennedy, T., Klaproth, M., Kolleck, M., Koller, S., Kotsialos, E., Kraaikamp, E., Langer, P., Lawrenson, A., Le Clech', J.-C., Lenaerts, C., Liebecq, S., Linder, D., Long, D.M., Mampaey, B., Markiewicz-Innes, D., Marquet, B., Marsch, E., Matthews, S., Mazy, E., Mazzoli, A., Meining, S., Meltchakov, E., Mercier, R., Meyer, S., Monecke, M., Monfort, F., Morinaud, G., Moron, F., Mountney, L., Müller, R., Nicula, B., Parenti, S., Peter, H., Pfiffner, D., Philippon, A., Phillips, I., Plessier, J.-Y., Pylyser, E., Rabecki, F., Ravet-Krill, M.-F., Rebellato, J., Renotte, E., Rodriguez, L., Roose, S., Rosin, J., Rossi, L., Roth, P., Rouessel, F., Roulliy, M., Rousseau, A., Ruane, K., Scanlan, J., Schlatter, P., Seaton, D.B., Silliman, K., Smit, S., Smith, P.J., Solanki, S.K., Spescha, M., Spencer, A., Stegen, K., Stockman, Y., Szvec, N., Tamiatto, C., Tandy, J., Teriaca, L., Theobald, C., Tychon, I., van Driel-Gesztelyi, L., Verbeeck, C., Vial, J.-C., Werner, S., West, M.J., Westwood, D., Wiegmann, T., Willis, G., Winter, B., Zerr, A., Zhang, X., Zhukov, A.N.: 2020, The Solar Orbiter EUV instrument: The Extreme Ultraviolet Imager. *Astron. Astrophys.* **642**, A8. DOI ADS.
- Rottman, G.: 2005, The SORCE Mission. *Sol. Phys.* **230**, 7. DOI ADS.
- Rottman, G.J., Woods, T.N., Sparn, T.P.: 1993, Solar-Stellar Irradiance Comparison Experiment 1. I - Instrument design and operation. *J. Geophys. Res.* **98**, 10,667. DOI ADS.
- Roussel-Dupre, D.: 1983, H I Lyman-alpha in the sun - The effects of partial redistribution in the line wings. *Astrophys. J.* **272**, 723. DOI ADS.
- Rubio da Costa, F., Fletcher, L., Labrosse, N., Zuccarello, F.: 2009, Observations of a solar flare and filament eruption in Lyman α and X-rays. *Astron. Astrophys.* **507**, 1005. DOI ADS.
- Shimizu, T., Imada, S., Kawate, T., Ichimoto, K., Suematsu, Y., Hara, H., Katsukawa, Y., Kubo, M., Toriumi, S., Watanabe, T., Yokoyama, T., Korendyke, C.M., Warren, H.P., Tarbell, T., De Pontieu, B., Teriaca, L., Schühle, U.H., Solanki, S., Harra, L.K., Matthews, S., Fludra, A., Auchère, F., Andretta, V., Naletto, G., Zhukov, A.: 2019, The Solar-C EUVST mission. In: Siegmund, O.H. (ed.) *UV, X-Ray, and Gamma-Ray Space Instrumentation for Astronomy XXI, Society of Photo-Optical Instrumentation Engineers (SPIE) Conference Series* **11118**, 1111807. DOI ADS.
- Simões, P.J.A., Reid, H.A.S., Milligan, R.O., Fletcher, L.: 2019, The Spectral Content of SDO/AIA 1600 and 1700 Å Filters from Flare and Plage Observations. *Astrophys. J.* **870**, 114. DOI ADS.
- Snow, M., McClintock, W.E., Woods, T.N., Elliott, J.P.: 2022, SOLar-STellar Irradiance Comparison Experiment II (SOLSTICE II): End-of-Mission Validation of the SOLSTICE Technique. *Sol. Phys.* **297**, 55. DOI ADS.
- Vernazza, J.E., Avrett, E.H., Loeser, R.: 1973, Structure of the Solar Chromosphere. Basic Computations and Summary of the Results. *Astrophys. J.* **184**, 605. DOI ADS.
- Vernazza, J.E., Avrett, E.H., Loeser, R.: 1981, Structure of the solar chromosphere. III. Models of the EUV brightness components of the quiet sun. *Astrophys. J.* **45**, 635. DOI ADS.
- Watanabe, T.: 2014, The Solar-C Mission. In: Oschmann, J. Jacobus M., Clampin, M., Fazio, G.G., MacEwen, H.A. (eds.) *Space Telescopes and Instrumentation 2014: Optical, Infrared, and Millimeter Wave, Society of Photo-Optical Instrumentation Engineers (SPIE) Conference Series* **9143**, 914310. DOI ADS.
- Wauters, L., Dominique, M., Milligan, R., Dammasch, I.E., Kretschmar, M., Machol, J.: 2022, Observation of a Flare and Filament Eruption in Lyman- α on 8 September 2011 by the PROject for OnBoard Autonomy/Large Yield Radiometer (PROBA2/LYRA). *Sol. Phys.* **297**, 36. DOI ADS.
- Woods, T.N., Eparvier, F.G., Fontenla, J., Harder, J., Kopp, G., McClintock, W.E., Rottman, G., Smiley, B., Snow, M.: 2004, Solar irradiance variability during the October 2003 solar storm period. *Geophys. Res. Lett.* **31**, L10802. DOI ADS.
- Woods, T.N., Eparvier, F.G., Hock, R., Jones, A.R., Woodraska, D., Judge, D., Didkovsky, L., Lean, J., Mariska, J., Warren, H., McMullin, D., Chamberlin, P., Berthiaume, G., Bailey, S., Fuller-Rowell, T., Sojka, J., Tobiska, W.K., Viereck, R.: 2012, Extreme Ultraviolet Variability Experiment (EVE) on the Solar Dynamics Observatory (SDO): Overview of Science Objectives, Instrument Design, Data Products, and Model Developments. *Sol. Phys.* **275**, 115. DOI ADS.
- Wueller, J.-P., Lemen, J.R., Tarbell, T.D., Wolfson, C.J., Cannon, J.C., Carpenter, B.A., Duncan, D.W., Gradwohl, G.S., Meyer, S.B., Moore, A.S., Navarro, R.L., Pearson, J.D., Rossi, G.R., Springer, L.A., Howard, R.A., Moses, J.D., Newmark, J.S., Delaboudiniere, J.-P., Artzner, G.E., Auchere, F., Bougnnet, M., Bouyries, P., Bridou, F., Clotaire, J.-Y., Colas, G., Delmotte, F., Jerome, A., Lamare, M., Mercier, R., Mullet, M., Ravet, M.-F., Song, X., Bothmer, V., Deutsch, W.: 2004, EUVI: the STEREO-SECCHI extreme ultraviolet imager. In: Fineschi, S., Gummmin, M.A. (eds.) *Telescopes and Instrumentation for Solar Astrophysics, Society of Photo-Optical Instrumentation Engineers (SPIE) Conference Series* **5171**, 111. DOI ADS.
- Xu, Y., Tian, H., Hou, Z., Yang, Z., Gao, Y., Bai, X.: 2022, Sun-as-a-star Spectroscopic Observations of the Line-of-sight Velocity of a Solar Eruption on 2021 October 28. *Astrophys. J.* **931**, 76. DOI ADS.
- Zhang, Z., Chen, D.-Y., Wu, J., Chang, J., Hu, Y.-M., Su, Y., Zhang, Y., Wang, J.-P., Liang, Y.-M., Ma, T., Guo, J.-H., Cai, M.-S., Zhang, Y.-Q., Huang, Y.-Y., Peng, X.-Y., Tang, Z.-B., Zhao, X., Zhou, H.-H., Wang, L.-G., Song, J.-X., Ma, M., Xu, G.-Z., Yang, J.-F., Lu, D., He, Y.-H., Tao, J.-Y., Ma, X.-L., Lv, B.-G., Bai, Y.-P., Cao, C.-X., Huang, Y., Gan, W.-Q.: 2019, Hard X-ray Imager (HXI) onboard the ASO-S mission. *Research in Astronomy and Astrophysics* **19**, 160. DOI ADS.